Journal of Power Sources 285 (2015) 266–273

Contents lists available at ScienceDirect

Journal of Power Sources

journal homepage: www.elsevier.com/locate/jpowsour

# Heat generation rate measurement in a Li-ion cell at large C-rates through temperature and heat flux measurements

S.J. Drake [a], M. Martin [b], D.A. Wetz [b], J.K. Ostanek [c], S.P. Miller [c], J.M. Heinzel [c], A. Jain [a, *]

[a] Mechanical and Aerospace Engineering Department, University of Texas at Arlington, USA
[b] Electrical Engineering Department, University of Texas at Arlington, USA
[c] Naval Surface Warfare Center, Carderock Division, U.S. Navy, USA

## HIGHLIGHTS

- Presents experimental method for heat generation measurement in Li-ion cells.
- Method is based on temperature and heat flux measurement.
- Experimental data agrees with well-established theoretical models.
- A novel method for indirect measurement of internal temperature is also presented.
- Results may contribute towards thermal safety of Li-ion cells.

## GRAPHICAL ABSTRACT

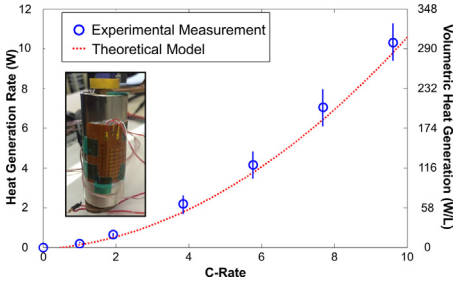


## ARTICLE INFO

*Article history:*
Received 13 January 2015
Received in revised form
13 February 2015
Accepted 1 March 2015
Available online 4 March 2015

*Keywords:*
Lithium-ion batteries
Heat generation rate measurement
Heat flux sensor
Thermal conduction
Battery safety

## ABSTRACT

Understanding the rate of heat generation in a Li-ion cell is critical for safety and performance of Li-ion cells and systems. Cell performance, cycle life, and system safety all depend on temperature distribution in the cell, which, in turn, depends on heat generation rate within the cell and on heat removal rate at the cell surface. Despite the existence of a number of theoretical models to predict heat generation rate, there is not much literature on experimental measurement at high C-rates. This paper reports measurement of heat generation rate from a Li-ion cell at high discharge rates, up to 9.6C, using measurements of cell temperature and surface heat flux. As opposed to calorimetry-based approaches, this method can be applied *in situ* to yield measurements of heat generation rate in laboratory or field use provided that at least one *a priori* test is performed to measure the temperature gradient within a cell in the same ambient condition. This method is based on simultaneous determination of heat stored and heat lost from the cell through heat flux and temperature measurements. A novel method is established for measurement of the internal temperature of the cell. Heat generation measurements are shown to agree with well-established theoretical models. The effect of actively cooling the cell is briefly discussed.



## 1. Introduction

Lithium-ion cells [1,2] have been investigated for a variety of energy storage and conversion processes in several applications [3–5]. The process of conversion of electrical energy to chemical energy and vice versa inherently produces heat [6–9], which results in increased cell temperature [10–12]. The operation of a Lithium-ion cell is based on several highly coupled phenomena involving multiple physical processes. For example, exothermic electrochemical reactions produce heat [6,9,13], which causes

* Corresponding author. 500 W First St, Rm 211, Arlington, TX 76019, USA.
*E-mail address:* jaina@uta.edu (A. Jain).

http://dx.doi.org/10.1016/j.jpowsour.2015.03.008
0378-7753/

temperature rise. Since temperature directly affects the rates of electrochemical reactions and electrical impedances [6], the thermal performance of the cell in turn affects electrochemical and electrical performance.

Uncontrolled temperature rise in a Li-ion cell is known to adversely affect performance as well as safety [14,15]. Power fade, capacity fade and self-discharge are well known performance-related problems at high temperature [5,15–17]. In addition, safety at high temperature is a major concern [18,19]. A series of exothermic reactions feeding into each other are known to occur if the cell temperature exceeds a certain threshold [20]. This thermal runaway is a serious concern that may lead to catastrophic failure.

Prediction of Li-ion cell temperature has been addressed by a number of papers, including analytical/numerical modeling [10–12,21–23], as well as temperature measurements [10,11,22,23]. Temperature measurement has been mostly limited to measuring the outside surface temperature, although some indirect measurements of the core temperature have also been reported [22,24]. Significant temperature gradient exists within the cell, particularly at high currents, due to the low radial thermal conductivity of the cell [10,24].

Temperature rise in a Li-ion cell during operation is governed by three processes: the rate at which heat is generated within the cell, the rate at which heat conducts within the cell to the outer surface, and the rate at which heat is removed from the cell outer surface to the surroundings. Heat dissipation to the ambient depends on the cell geometry and the cooling system performance. Heat conduction within the cell depends on thermal transport properties of the Li-ion cell, namely thermal conductivity and heat capacity [25]. A few papers have reported measurements of these properties. Heat capacity of batteries has been measured [26]. Measurement of thermal conductivity and heat capacity of Li-ion cells using xenon flash technology (XFT) and steady-state measurements have been reported [27]. Recent measurements of thermal properties of a Li-ion cell using an external heating method indicate strong anisotropy in thermal conduction between radial and axial directions [25,28]. The radial thermal conductivity is markedly lower than axial conductivity for spiral-wound cell designs.

In addition to heat conduction within the cell and heat removed at the cell surface, an understanding of internal heat generation rate is also important for a complete thermal understanding of a cell. A number of papers have presented theoretical analysis of heat generation rate as a function of electrochemical parameters such as C-rate [6,7,9]. Heat generation is caused by several different mechanisms, including exothermic heats of reaction, Ohmic losses, etc. A widely used theoretical model predicts the heat generation rate as follows [6].

$$Q_{theoretical} = I\cdot(U - V) - I\cdot T\frac{\partial U}{\partial T} \quad (1)$$

Where I, V and T are current, voltage and temperature, respectively, and U is the open circuit voltage corresponding to the depth of discharge. The first term in Equation (1) accounts for heat generation due to electrochemical overpotentials, whereas the second term accounts for entropic heat generation, or the reversible heat of reaction of the overall electrochemical reaction. Some authors also refer to a time-based heat of mixing, which accounts for temperature variation due the changes in local concentrations of dissolved specials. The latter, occurring as a transient phenomenon, has not been well characterized for lithium ion cells and is generally neglected in practice. Further, heat generation due to side reactions is also generally neglected in theoretical models.

There are relatively few studies which report experimental measurements of heat generation, especially *in situ* measurements. A few papers have reported measurement of various electrochemical sources of heat generation, such as overpotential and entropy sources by measuring a number of electrical parameters and their temperature dependence [29,30]. Comparison of heat generation rates determined using such sources with experimental measurements has been presented. Most literature on heat generation measurement addresses measurements low C-rates processes, typically C/1 or lower [14,31,32] that are commonly found in consumer electronics but not in other, more aggressive applications. Some high-rate measurements have been reported [33], but the calorimetry-based methods require enclosing the cell in a calorimeter apparatus. Calorimetry-based experiments are also typically expensive and may not be readily available for field use. It is clearly desirable to develop real-time measurement methods for high C-rate processes that can be implemented in realistic conditions.

This paper reports *in situ* measurements of heat generation rate during high-rate discharge of a cylindrical Li-ion cell, up to 9.6C. These measurements utilize heat flux and temperature sensor measurements such that heat generation rate measurements are based on the thermal response of the cell, as opposed to other methods based on electrical measurements such as cell potential and current [6,7]. Heat stored in the cell and heat lost through the outside surfaces – two independent components of the total heat generated – are measured simultaneously. To do so, the internal temperature of the cell during discharge is estimated using a novel method. The heat generation rate is found to have a quadratic dependence on C-rate, and is in good agreement with estimates based on the theoretical model represented by Equation (1). Experiments are carried out with and without active cooling by a fan. Results indicate that the presence of active cooling increases the heat loss component and reduces the heat storage component, while the total heat generated remains largely unchanged.

The next section discusses the experimental method used for the measurements. Experimental setup is discussed in Section 3. Measurement results are presented in Section 4.

## 2. Method for heat generation rate measurement

Consider a charge or discharge process for a Li-ion cell, starting at t = 0, during which heat is generated. Let Q(t) be the total heat generated, in Joules, up to time t. As shown in Fig. 1(a), Q(t) is either stored within the cell, $Q_A(t)$, or is lost to the ambient through the outer surface of the cell, $Q_B(t)$. The component $Q_A(t)$ results in temperature rise of the cell, whereas $Q_B(t)$ results in an increase in the heat flux leaving the cell at the outer surface. $Q_A(t)$ is related to the volume-averaged cell temperature rise as follows:

$$Q_A(t) = \rho \forall C_p \Delta T_{volavg}(t) \quad (2)$$

where ρ, $C_p$, and ∀ are the mass density, heat capacity and total volume of the cell respectively, assumed to remain constant throughout the experiment, which is reasonable due to the relatively small temperature range during the experiments (room temperature to about 60 °C). $\Delta T_{volavg}(t)$ is the volume-averaged cell temperature rise at any time, t. Thus, a measurement of $\Delta T_{volavg}(t)$ can be combined with cell thermal properties to determine $Q_A(t)$. Note that due to significant temperature gradients within the cell [10,24], the cell is not characterized by a single temperature, and a volume-averaged temperature rise is needed for equation (2).

On the other hand, $Q_B(t)$, the component corresponding to heat lost through the outer surface, can be measured using a heat flux sensor. A heat flux sensor outputs a DC voltage proportional to the heat flux passing normal to the sensor surface at any time. Thus, $Q_B(t)$ is given by

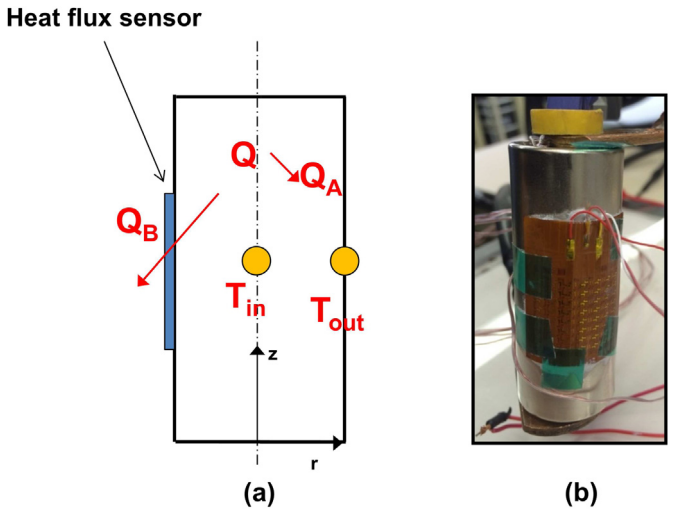


**Fig. 1.** (a) Schematic of stored and lost components of total heat generated, (b) Picture showing Li-ion cell under test, including a heat flux sensor.

$$Q_B(t) = \int_0^t C \cdot V_{HFS}(\tau) \cdot A d\tau \tag{3}$$

where $V_{HFS}(\tau)$ is the voltage output of the heat flux sensor at any time $\tau$, C is the calibration constant of the heat flux sensor ($Wm^{-2}\ V^{-1}$) which connects the measured voltage difference across the sensor with the heat flux passing through it, and A is the cell surface area. The value of C for the specific heat flux sensor used is 2.1 $Wm^{-2}\ V^{-1}$.

The total heat generated is then simply given by

$$Q(t) = Q_A(t) + Q_B(t) \tag{4}$$

The instantaneous heat generation *rate*, in Watts, can be determined by differentiating the experimentally measured Q as a function of time.

Equations (2)–(4) represent a heat generation measurement method which relies only on measured thermal responses in an operating Li-ion cell, as opposed to estimating the heat generation rate from cell voltage and current. Measurements of only temperature and heat flux are needed, and no information is needed about the underlying mechanisms or processes responsible for heat generation in the cell. As discussed later in this section, these measurements can be carried out *in situ* while the cell charges/discharges in realistic conditions.

In general, $\Delta T_{volavg}(t)$ is given by

$$\Delta T_{volavg}(t) = \frac{2}{R^2 H} \int_0^H \int_0^R r \Delta T(r,z,t) dr dz \tag{5}$$

Determination of $\Delta T_{volavg}(t)$ requires measurement of temperature rise throughout the internal volume of the cell, followed by integration according to Equation (5). This has limited practicality and is generally limited to controlled, laboratory testing [34]. However, it is shown in Appendix A that within the parameter space encountered in these experiments, the volume-averaged temperature rise in a cylinder can be determined from only two temperature measurements as follows:

$$\Delta T_{volavg}(t) \approx \Delta T_{mean}(t) = \frac{\Delta T_{core}(t) + \Delta T_{out}(t)}{2} \tag{6}$$

where $\Delta T_{core}(t)$ and $\Delta T_{out}(t)$ are the temperature rise at the core of the cell (r = 0), and at the outside surface of the cell (r = R) at mid-height respectively.

A further difficulty in the determination of $\Delta T_{volavg}(t)$ lies in the measurement of the core temperature $\Delta T_{core}(t)$. While a few papers have reported direct measurement of $\Delta T_{core}(t)$ using internal thermocouples [22,23], this may not always be possible. An indirect method for determination of the cell core temperature is utilized in this paper. This method is based on measuring the core and outside temperatures of a *drilled* cell having the same geometry and thermal properties, undergoing discharge in the same ambient condition as the *undrilled* cell of interest. Appendix B uses the theory of thermal conduction to show that the core temperature of an undrilled cell, $\Delta T_{core,undrilled}(t)$ is given by

$$\Delta T_{core,undrilled}(t) = \Delta T_{core,drilled}(t) \times \frac{\Delta T_{out,undrilled}(t)}{\Delta T_{out,drilled}(t)} \tag{7}$$

In short, Equation (7) states that the ratio of the core and outside temperatures is the same for the drilled and undrilled cells, assuming same geometry, thermal properties, and ambient conditions. Heat generation rates in the two cells do not need to be the same, although the ambient conditions must be identical between the *a priori* (drilled cell) experiments and the *in situ* (undrilled cell) experiments. Equation (7) makes it possible to use a one-time, *a priori* measurement of the core temperature of a drilled cell to non-invasively determine the core temperature of a similar undrilled cell undergoing any charge/discharge process. Once the core temperature is determined, Equations (2) and (6) are used to determine the heat stored in the cell. Finally, Equation (4) is used to determine heat generated in the cell. This measurement can be carried out at any time during the cell discharge process, and hence can provide heat generated, in Joules, as a function of time. The instantaneous and time-averaged heat generation rates, in Watts, can also be determined by numerical differentiation of the experimental data.

## 3. Experimental method

A previously unused 2.6 Ah $LiFePO_4$ 26650 cell is used in the measurements. Prior to heat generation measurements, Electrochemical Impedance Spectroscopy (EIS) of the cell is performed using a Princeton Applied Research PARSTAT 4000 potentiostat. The equivalent series resistance (ESR) of the cell is measured to be 12.0 mΩ. An EIS measurement prior to heat generation measurements establishes the electrical health of the cell being used in the measurements.

The fully charged cell is connected to a Maccor Series 4000 testing system that incorporates electrical loads and power supplies to charge and discharge the cell at a desired rate. The Maccor system also provides voltage and current measurements. Measurements from T-type thermocouples attached to the cell are monitored to ensure that the cell is uniformly at room temperature prior to any discharge. A maximum operating temperature of 55 °C is implemented during the discharge process for safety.

Fig. 1(b) shows the test cell, including a heat flux sensor attached on the outer surface. A HFS-4 heat flux sensor from Omega Engineering is placed in direct contact with the outer surface of the cell using Omegatherm-201 thermal paste, to ensure good thermal contact with the cell, and Kapton polyimide tape, to help secure the sensor to the cell. The heat flux sensor incorporates a dual-layered thermocouple array to output a voltage signal that is proportional

to the heat flux passing through the sensor surface. Sensor output is measured using a National Instruments NI-9213 16-channel thermocouple input module inside a NI cDAQ 9171 single slot USB chassis. A single input channel is configured to log data in the microvolt range. T-type thermocouples are also placed in contact with the outer surface to measure $T_{out}(t)$. Additional channels in the same NI cDAQ 9171 are configured for use with these thermocouples. It is used in conjunction with an NI LabVIEW VI for data acquisition from thermocouples. Temperature and heat flux measurements are recorded every second for the entire discharge duration. The top and bottom axial surfaces of the cell are insulated, so that the surface area A in Equation (3) refers to only the curved surface area.

A set of experiments are carried out to evaluate the effect of active cooling on the thermal performance of the cell. In these experiments, air is blown over the outer surface of the cell by a Holmes two-speed personal fan with air speed of 3.6 m/s.

$\Delta T_{core,drilled}(t)$, which is needed to determine $\Delta T_{core,undrilled}(t)$ using Equation (6) is measured using a separate, identical 26650 Li-ion cell. A 7/32-in hole is drilled through the cap of this cell. Three K-type thermocouples are aligned vertically and encased in a thin-walled heat shrink tubing. This allows for better placement accuracy and minimizes unwanted shifting during assembly. The tubing carrying the thermocouples is inserted down the spindle gap of the cell. The hole in the cell cap is then back-filled with an OmegaBond two part thermal epoxy. The entire process is carried out within an inert gas glovebox environment. The cell is cured overnight in the glovebox. Fig. 2 shows images of the thermocouples mounted on the tubing, as well as the drilled hole in the cell. Prior to heat generation measurement, the cell is re-characterized through an EIS measurement. Cell ESR is found to undergo minimal change (from 12.0 mΩ to 14.0 mΩ). This indicates that the cell is still capable of storing charge with negligible change in its electrical characteristics.

The mass density of the test cell is determined separately by measuring its volume using Vernier calipers and its weight using a sensitive scale balance. The value of heat capacity of the cell, to be used in Equation (2) is obtained from a Hot Disk Transient Plane Source (TPS) method based measurement.

## 4. Results and discussion

### 4.1. Temperature and heat flux measurements

Following EIS characterization, the 26650 Li-ion cell is discharged at six different discharge currents, ranging from 2.6A (1C) to 25A (9.6C). Fig. 3 plots core and outside surface temperatures for the drilled and undrilled cell as a function of time during 15A (5.8C) discharge. Plots similar for Fig. 3 are obtained for discharge at other

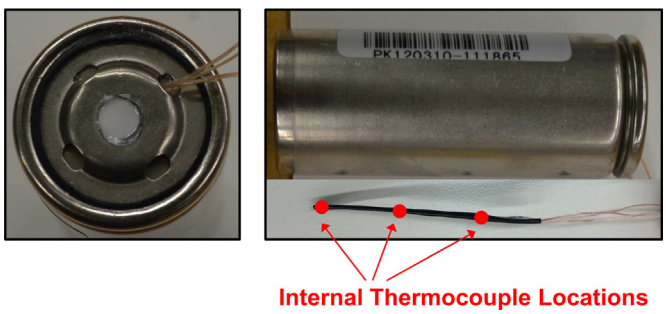


**Fig. 2.** Pictures showing top and side views of the drilled Li-ion cell. Approximate locations of thermocouples are shown in side view.

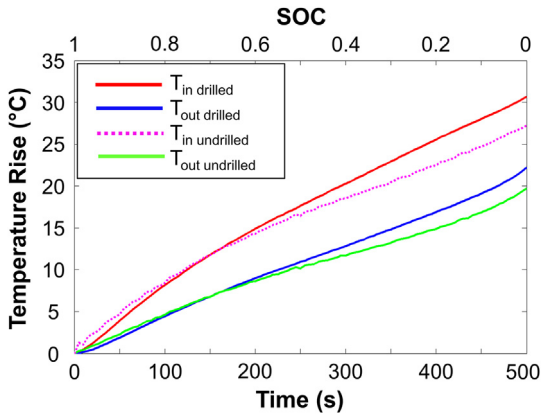


**Fig. 3.** Core and outside temperatures as function of time during 15A (5.8C) discharge for undrilled and drilled cell.

C-rates as well.

Note that the core temperature of the undrilled cell is obtained from other measurements using linear scaling described in Appendix B. To further investigate this method, the computed core temperature is compared with the transient temperature profile predicted by a recently developed transient thermal model in Fig. 4 [11]. This model solves the governing energy conservation equations to predict the temperature field as a function of time. The two follow similar trends for each C-rate investigated here. This small discrepancy between the two is due to the use of the average heat generation rate in the transient thermal model, whereas in reality, the heat generation rate may not be uniform in time. As a result, the transient model curves are smooth, while the experimental curves are not. In both cases, however, the total heat generation during the entire discharge process is similar.

### 4.2. Measurement of components of heat generation

Temperature and heat flux measurements outlined above are used to determine the heat lost, heat stored and total heat generated as functions of time for each C-rate. Fig. 5 shows a representative plot of these quantities as functions of time during 15A (5.8C) discharge. Most of the heat generated in the cell during the discharge process is stored within. This is consistent with the lack of any active cooling of the cell. In all, about 2100 J heat is

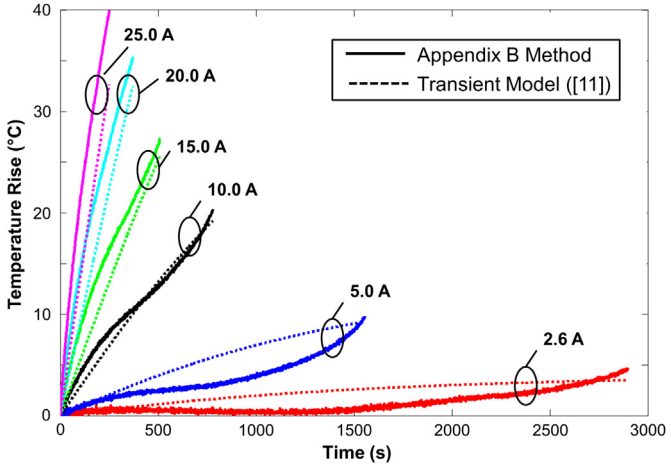


**Fig. 4.** Comparison of the prediction of internal temperature with a transient thermal model.

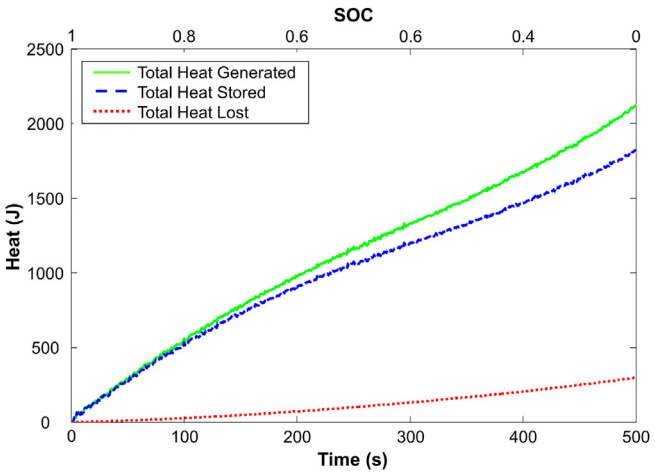


**Fig. 5.** Measured heat stored, heat lost and heat generated as functions of time for an uncooled cell at 15A (5.8C) discharge.

generated, which is about 8% of the 26200 J energy converted from chemical to electrical form during the discharge process. Plots similar to Fig. 5 are obtained for other C-rates.

### 4.3. Heat generation and heat generation rate as functions of C-rate

Fig. 6 plots total heat generated for the entire discharge process as a function of time for six different discharge currents. There appears to be more rapid heat generation towards the end of the discharge process, although for larger C-rates, heat generation is nearly linear with time. As expected, Fig. 6 shows that low C-rate discharge results in significantly lower heat generated over a longer time period. Note that for the 25A discharge case, the cell temperature reached the 55 °C safety limit before completion of the discharge process. As a result, a portion of the 25A curve, shown as a broken line on Fig. 6 is extrapolated based on actual measurements.

The average heat generation rate over the entire discharge period is computed, and plotted as a function of C-rate in Fig. 7, which shows strong dependence on C-rate. This data fits well with a quadratic curve, which is expected, based on the $I^2$ dependence of heat generation mechanisms within the cell. The heat generation rate at 9.6C, the highest C-rate tested in this work is 10.6W for a single 26650 cell. Expressed as volumetric heat generation rate, this corresponds to 307 W/L.

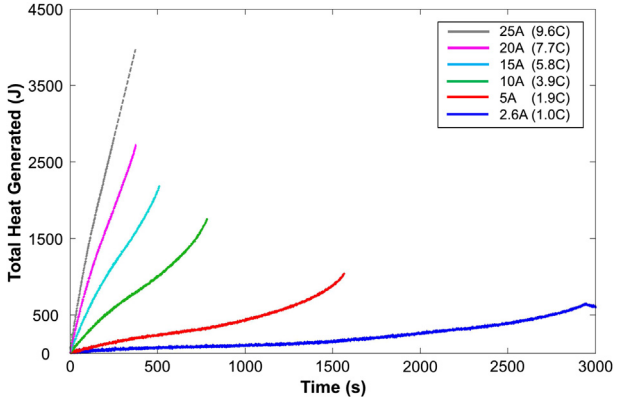


**Fig. 6.** Heat generated as a function of time for different C-rates.

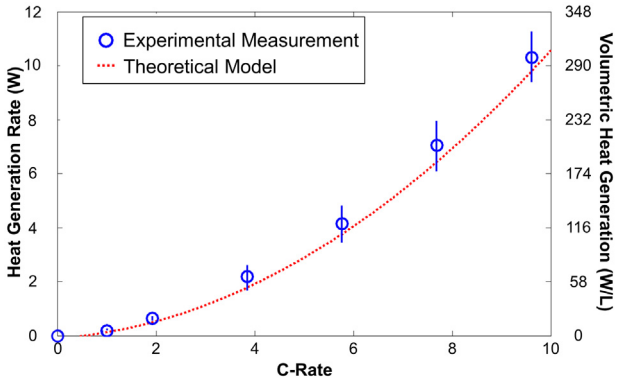


**Fig. 7.** Experimentally measured heat generation rate as a function of C-rate, and comparison with theoretical model.

### 4.4. Comparison with theoretical model

The commonly used heat generation model for Li-ion cells, given by Equation (1) is used to compute the heat generation rate and compare with experimental data. In this model, I and V, the current and voltage across the cell are based on measurements during tests. The open-circuit voltage, U, is determined by plotting the experimentally measured voltage as a function of discharge current at each SOC during the discharge process. This curve is found to be linear for all experiments, and extrapolation to zero current results in determination of U. The volume averaged cell temperature defined in Equation (5) is determined using Equation (6) for use in the entropic heating term in Equation (1). Finally, the dU/dT term in Equation (1) is obtained from measuring open-circuit voltage response to step-changes in temperature at various SOC similar to the procedures described by Forgez et al. [22]. The entropic heating term in Equation (1) is endothermic from fully charged state to an SOC of around 35%, and exothermic below an SOC of 35%. The entropic heating term contributes to the non-linear heat generation curves at lower discharge rates shown in Fig. 6, while the entropic heating term becomes less significant at higher discharge rates.

The heat generation rate predicted by Equation (1) is compared with the theoretical calculation in Fig. 7. Experimental data and theoretical calculation agree with each other within experimental uncertainty. While the theoretical curve is based on an analytical model that relates heat generation rate to electrical and electrochemical parameters such as current and voltage, the experimental curve represents a purely thermal, *in situ* measurement of the heat generation rate. There is greater deviation as a percentage between the two at lower C-rates, where there is larger relative uncertainty in experimental measurements due to the small magnitude of heat generation rate being measured. The dominant sources of uncertainty in experimental measurement include heat loss through metal tabs used for electrical contact, and voltage measurement accuracy of the NI-9213 DAQ. Other less significant sources of uncertainty include uncertainty in measurements of temperatures, currents and voltages, heat loss down the thermocouple wires, etc. In particular, uncertainty in current and voltage measurement is less than 0.5%. Note that the heat flux sensor itself adds a thermal resistance and capacitance. However, due to the small mass of the heat flux sensor, its thermal resistance is found to be very small compared to that of the cell itself. Similarly, due to the small thickness of the heat flux sensor, its thermal resistance to heat flux is also negligible compared to thermal resistance due to convective heat loss from the cell surface. Both effects are found to be less than 1%, and hence negligible.

### 4.5. Energy conversion efficiency

Any heat generated during the discharge process results in reduction in the efficiency of energy conversion from chemical to electrical form. This energy conversion efficiency may be defined as

$$\eta = \frac{E_{elec}}{E_{elec} + Q} \tag{8}$$

where $E_{elec}$ is the electrical work output.

Efficiency, η, is plotted as a function of C-rate in Fig. 8. The energy conversion efficiency reduces as C-rate increases, due to the increased heat generation rate at large C-rates.

### 4.6. Effect of cell drilling on heat generation rate

As discussed in Section 2, determination of core temperature of the baseline, undrilled cell requires one-time drilling and insertion of a thermocouple into one separate cell. Experiments are also carried out to determine the effect of drilling the cell on heat generation rate. The heat generation rate in the drilled cell is measured at a number of C-rates using the same methodology as the undrilled cell. Fig. 9 compares heat generation rate at different C-rates for the undrilled and drilled cells. Both curves follow the expected quadratic behavior. There is a slight increase in heat generation rate as a result of drilling the cell. At 25A, the highest discharge current tested, the heat generation rate increased from 10.5W in the undrilled cell to 12.0W in the drilled cell. This is consistent with EIS measurements that indicate a small increase in cell ESR due to drilling.

### 4.7. Effect of active cooling

Heat generation measurement experiments are repeated in the presence of active cooling using a fan. All other experimental conditions are maintained to be the same as the baseline case on an uncooled undrilled cell. Experiments are carried out at a number of C-rates. Fig. 10 plots the heat stored, heat lost and total heat generated in the cell during 15A (5.8C) discharge as a function of time while being actively cooled. In comparison with Fig. 5, where these data are plotted for the baseline, uncooled cell, there is greater heat lost and lesser heat stored. This is consistent with the presence of active cooling that facilitates greater heat removal, and hence reduced heat stored. Despite the relative changes in heat lost and heat stored, heat generated – which is the sum of the two – is measured to be nearly the same as the uncooled case. Similar behavior is also observed at other C-rates.

Fig. 11 compares the overall, average heat generation rate between uncooled and cooled cells at different C-rates. Data from these two cases are very close to each other for each C-rate, indicating that while cooling results in reduced heat stored within the cell – and hence reduced cell temperature – the overall heat generation rate remains relatively unaffected by the cooling. Curves for both cases fit well by a quadratic equation, as expected.

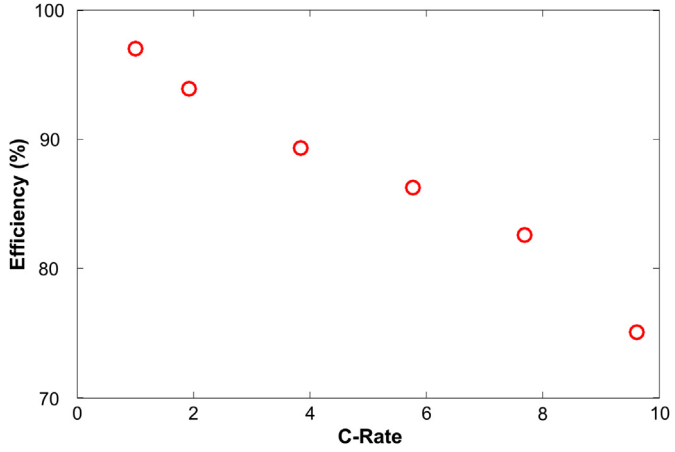


**Fig. 8.** Efficiency of energy conversion as a function of C-rate.

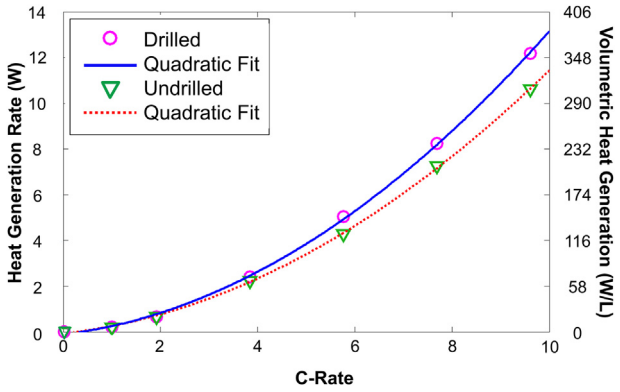


**Fig. 9.** Comparison of heat generation rate as a function of C-rate for undrilled and drilled cells.

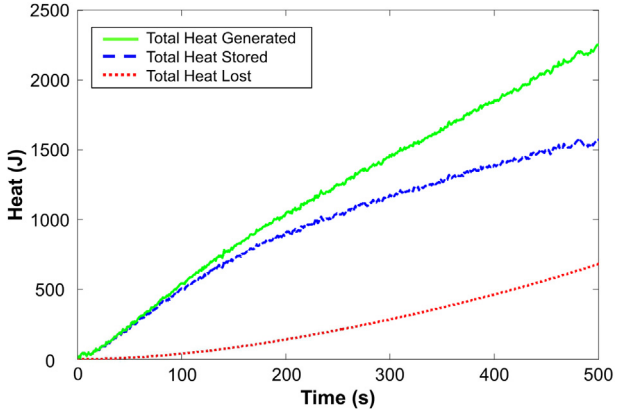


**Fig. 10.** Measured heat stored, heat lost and heat generated as functions of time for a cooled cell at 15A (5.8C) discharge.

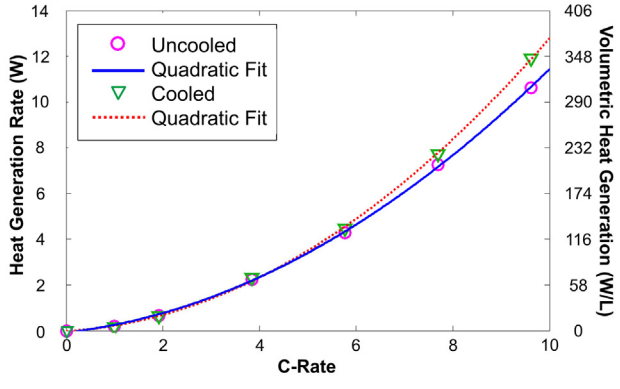


**Fig. 11.** Comparison of measured heat generation rate as a function of C-rate for uncooled and cooled cells.

## 5. Conclusions

This paper presents *in situ* measurement of heat generation rate based on the measured thermal response of a Li-ion cell under discharge at high C-rates. Specifically, the method is based on measurement of heat stored in the cell, and heat lost to the ambient and does not rely on the specific mechanisms underlying heat generation in the cell. The method utilizes a novel result from the theory of thermal conduction to determine the volume-averaged cell temperature from only two discrete, point measurements, and to determine the internal temperature of an undrilled cell from one-time measurements on a similar, drilled cell. Experimental data are in excellent agreement with well-known theoretical models for heat generation rate in cells. Results indicate a strong C-rate dependence of heat generation, as expected. The measurement method and data presented here contribute towards the fundamental understanding of thermal phenomena in Li-ion cells, as well as effective thermal management strategies for reducing operating temperature for Li-ion cells, thereby improving safety, reliability and performance.

## Acknowledgments

This work was supported under ONR grant numbers N000141310819 and N000141410846.

## Appendix A. Determination of volume-averaged temperature rise of a cell

This appendix establishes that the volume-averaged temperature rise in a heat-generating cell can be obtained from the average of the temperature rise at the core of the cell and at the outer surface.

A finite-element transient thermal simulation is carried out for the discharge process with parameters representative of the experiments discussed in this paper. A 26650 Li-ion cell generating 6W heat is modeled. Radial and axial thermal conductivities of the cell are assumed to be 0.2 W/mK and 30 W/mK, based on recent measurements [25]. Two values of the convective heat transfer coefficient for the outer surface are considered – 10 W/m$^2$K and 100 W/m$^2$K. These values account for the natural convection and air cooled conditions in which the experiments are carried out. Uniform heat generation in the cell is assumed. While the heat generation rate in a cell may be non-uniform in general, due to temperature dependence of heat-generation mechanisms, the assumption of neglecting this non-uniformity results in good agreement of experimental data with models. Grid refinement is carried out in order to ensure grid independence of simulation results. The volume-averaged temperature $\Delta T_{volavg}$ as well as the mean of the outer and inner temperatures at mid-height, $\Delta T_{core}(t)$ and $\Delta T_{out}(t)$, are monitored as functions of time. As shown in Fig. A.1, there is close agreement between $\Delta T_{volavg}$ and the mean of $\Delta T_{core}$ and $\Delta T_{out}$ during the entire discharge process. Fig. A.1 also shows this comparison for a larger value of the convective heat transfer coefficient. There is somewhat greater deviation between $\Delta T_{volavg}$ and the mean of $\Delta T_{core}$ and $\Delta T_{out}$ as the convective heat transfer coefficient increases, due to the increased value of the Biot number. However, within the experimental conditions used in this paper, the approximation is reasonable, as shown in Fig. A.1.

This establishes that the volume averaged cell temperature can be reasonably approximated by the mean of temperature measurements at the core and outside surface of the cell at mid-height.

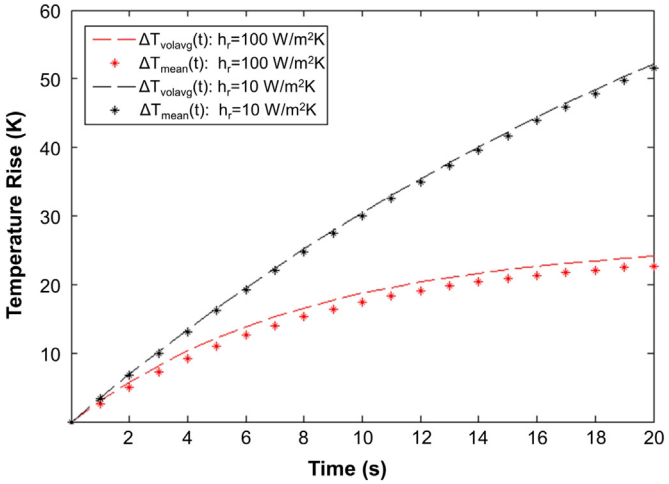


**Fig. A.1.** Comparison of $\Delta T_{volavg}(t)$ and $\Delta T_{mean}(t)$.

## Appendix B. Determination of core temperature of undrilled cell

In the temperature range of interest for Li-ion cell operation, the energy conservation equations governing thermal conduction within the cell are expected to be linear. In general, the transient temperature distribution in the cell in response to a uniform heat generation rate Q is given by

$$\Delta T(\bar{r}, t) = Q \cdot f(\bar{r}, k, \rho, C_p, t, geometry, BC) \tag{B.1}$$

where $\bar{r}$ is the spatial coordinate. The form of the function f is generally derived by solving the underlying governing energy conservation equations. BC refers to the imposed boundary conditions.

Now, consider two cells A and B of identical geometry and thermal properties, undergoing two different discharge processes with heat generation $Q_A$ and $Q_B$ respectively. Assume the same ambient conditions in both cases. Consider two locations $\bar{r}_{in}$ and $\bar{r}_{out}$ on the cells. Based on Equation (B.1) the temperatures at $\bar{r}_{in}$ and $\bar{r}_{out}$ for cell A are given by

$$\Delta T_A(\bar{r}_{in}, t) = Q_A \cdot f(\bar{r}_{in}, k, \rho, C_p, t, geometry, BC) \tag{B.2}$$

$$\Delta T_A(\bar{r}_{out}, t) = Q_A \cdot f(\bar{r}_{out}, k, \rho, C_p, t, geometry, BC) \tag{B.3}$$

Similarly, temperatures at $\bar{r}_{in}$ and $\bar{r}_{out}$ for cell B are given by

$$\Delta T_B(\bar{r}_{in}, t) = Q_B \cdot f(\bar{r}_{in}, k, \rho, C_p, t, geometry, BC) \tag{B.4}$$

$$\Delta T_B(\bar{r}_{out}, t) = Q_B \cdot f(\bar{r}_{out}, k, \rho, C_p, t, geometry, BC) \tag{B.5}$$

From Equations (B.2)–(B.5), it follows that

$$\frac{\Delta T_A(\bar{r}_{in}, t)}{\Delta T_A(\bar{r}_{out}, t)} = \frac{\Delta T_B(\bar{r}_{in}, t)}{\Delta T_B(\bar{r}_{out}, t)} \tag{B.6}$$

Thus, the ratio of temperatures at two locations at any time remains the same for two cells undergoing different discharge processes, as long as the geometry, thermal properties and boundary conditions remain the same. Application of this principle to a drilled cell and an undrilled cell results in Equation (7), which can be used to determine the core temperature of an undrilled cell without the need of inserting a thermocouple, as long as data from a one-time experiment on an identical drilled cell is available.

In order to experimentally validate the relationship between

internal and external temperatures represented by Equation (B.6), these temperatures are measured on a drilled cell undergoing discharge at various C-rates in either uncooled or cooled configuration. Fig. B.1 plots the ratio $\Delta T(\bar{r}_{in}, t)/\Delta T(\bar{r}_{out}, t)$ at two different discharge rates when the cell is uncooled. The ratio is found to stay nearly the same through the discharge process. Similar behavior is observed for the case when the cell is cooled with external flow, also shown in Fig. B.1. This shows that experimental data follows Equation (B.6) both when the cell is cooled and uncooled.

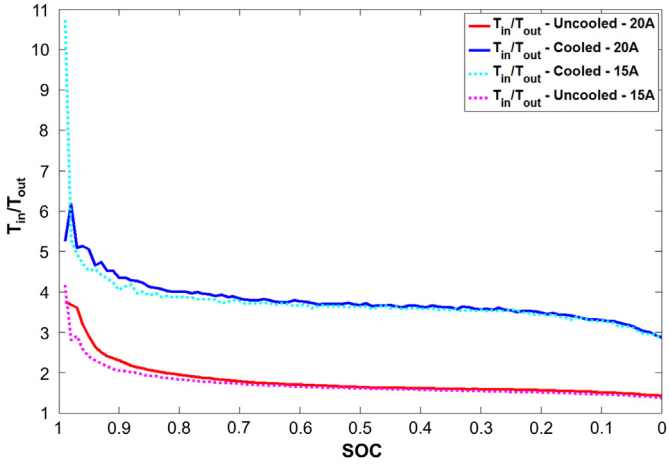


**Fig. B.1.** Experimental data on the ratio of core and external temperature for two different discharge charge in two different ambient conditions for validation of the model presented in Appendix B.

## References


[1] J. Goodenough, K. Park, J. Am. Chem. Soc. 135 (2013) 1167–1176.
[2] B. Scrosati, J. Garche, J. Power Sources 9 (2010) 2419–2430.
[3] A. Khaligh, Z. Li, IEEE Trans. Veh. Technol. 59 (2010) 2806–2814.
[4] R. Marsh, S. Vukson, S. Surampudi, B.V. Ratnakumar, M.C. Smart, M. Manzo, P.J. Dalton, J. Power Sources 97 (2001) 25–27.
[5] D. Linden, T.B. Reddy, Handbook of Batteries, third ed., McGraw-Hill, New York, 2002.
[6] K. Thomas, J. Newman, J. Power Sources 119 (2003) 844–849.
[7] D. Bernardi, E. Pawlikowski, J. Newman, J. Electrochem. Soc. 132 (1985) 5–12.
[8] Y. Yi, Y. Shi, N. Cai, J. Lee, X. He, J. Power Sources 199 (2012) 227–238.
[9] V. Srinivasan, C.Y. Wang, J. Electrochem. Soc. 150 (2003) A98–A106.
[10] K. Shah, S.J. Drake, D.A. Wetz, J.K. Ostanek, S.P. Miller, J.M. Heinzel, A. Jain, J. Power Sources 258 (2014) 374–381.
[11] K. Shah, S.J. Drake, D.A. Wetz, J.K. Ostanek, S.P. Miller, J.M. Heinzel, A. Jain, J. Power Sources 271 (2014) 262–268.
[12] P. Taheri, M. Yazdanpour, M. Bahrami, J. Power Sources 243 (2013) 280–289.
[13] Y. Chen, J.W. Evans, J. Electrochem. Soc. 143 (1996) 2708.
[14] T.M. Bandhauer, S. Garimella, T. Fuller, J. Electrochem. Soc. 158 (2011) R1–R25.
[15] M. Broussely, Aging mechanisms in Li-ion batteries and life prediction, in: W.A.V. Schalkwijk, B. Scrosati (Eds.), Advances in Lithium-ion Batteries, Kluwer Academic/Plenum Publishers, New York, 2002.
[16] D. Aurbach, B. Markovsky, G. Salitra, E. Markevich, Y. Talyossef, M. Koltypin, L. Nazar, B. Ellis, D. Kovacheva, J. Power Sources 165 (2007) 491.
[17] B. Johnson, R. White, J. Power Sources 70 (1998) 48.
[18] R. Spotnitz, J. Franklin, J. Power Sources 113 (2003) 81.
[19] D. Abraham, E. Roth, R. Kostecki, K. McCarthy, S. MacLaren, D. Doughty, J. Power Sources 161 (2006) 648.
[20] Q. Wang, P. Ping, X. Zhao, G. Chu, J. Sun, C. Chen, J. Power Sources 208 (2012) 210–224.
[21] W. Fang, O.J. Kwon, C.-Y. Wang, Int. J. Energy Res. 34 (2010) 107–115.
[22] C. Forgez, D.V. Do, G. Friedrich, M. Morcrette, C. Delacourt, J. Power Sources 195 (2010) 2961–2968.
[23] X. Lin, H. Perez, J. Siegel, A. Stefanopoulou, Y. Li, R. Anderson, Y. Ding, M. Castanier, IEEE Trans. Control Syst. Technol. 21 (2013) 1745–1755.
[24] R. Srinivasan, B. Carkhuff, M. Butler, A. Baisden, O. Uy, An external sensor for instantaneous measurement of the internal temperature in lithium-ion rechargeable cells, in: N. Dhar, P. Wijewarnasuriya, A. Dutta (Eds.), Energy Harvesting and Storage: Materials, Devices, and Applications, SPIE, 2011.
[25] S.J. Drake, D.A. Wetz, J.K. Ostanek, S.P. Miller, J.M. Heinzel, A. Jain, J. Power Sources 252 (2014) 298–304.
[26] A.A. Pesaran, M. Keyser, Thermal characteristics of selected EV and HEV batteries, in: Proc. Annual Battery Conf.: Advances & Applications, Long Beach, CA, USA, 2001.
[27] H. Maleki, S.A. Hallaj, J.R. Selman, R.B. Dinwiddie, H. Wang, J. Electrochem. Soc. 146 (1999) 947–954.
[28] J. Zhang, B. Wu, Z. Li, J. Huang, J. Power Sources 259 (2014) 106–116.
[29] K. Onda, H. Kameyama, T. Hanamoto, K. Ito, J. Electrochem. Soc. 150 (2003) A285–A291.
[30] K. Onda, T. Ohshima, M. Nakayama, K. Fukuda, T. Araki, J. Power Sources 158 (2006) 535–542.
[31] Y. Kobayashi, H. Miyashiro, K. Kumai, K. Takei, T. Iwahori, I. Uchida, J. Electrochem. Soc. 149 (2002) A978.
[32] H. Vaidyanathan, W. Kelly, G. Rao, J. Power Sources 93 (2001) 112.
[33] Y. Ye, L.H. Saw, Y. Shi, K. Somasundaram, A.A.O. Tay, Electrochim. Acta 134 (2014) 327–337.
[34] G. Zhang, L. Cao, S. Ge, C.-Y. Wang, C.E. Shaffer, C.D. Rahn, J. Electrochem. Soc. 161 (2014) A1499–A1507.